Electron impact dissociative excitation of O_2: 2. Absolute emission cross sections of the OI(130.4 nm) and OI(135.6 nm) lines

I. Kanik, C. Noren, O. P. Makarov, P. Vattipalle, and J. M. Ajello
Jet Propulsion Laboratory, California Institute of Technology, Pasadena, California, USA

D. E. Shemansky
Department of Aerospace and Mechanical Engineering, University of Southern California, Los Angeles, California, USA

Received 6 November 2000; revised 9 April 2003; accepted 23 April 2003; published 25 November 2003.

[1] In this work, we report the OI(135.6 nm) absolute emission cross section resulting from the long-lived (180 μs) OI($^5S \rightarrow {}^3P$) transition from dissociative excitation of O_2. From the ratio of the integrated intensities of the OI(135.6 nm) and OI(130.4 nm) features and from the absolute emission cross section for the OI(130.4 nm) emission feature from electron impact dissociative excitation of O_2 at 100 eV, the absolute emission cross section for the OI(135.6 nm) feature was determined to be 6.4×10^{-18} cm^2 at 100 eV. Electron impact-induced optical excitation functions for optically allowed transitions at 115.2 nm and 130.4 nm and for an optically forbidden transition at 135.6 nm were also obtained over the electron impact energy range 0–600 eV. The OI(135.6 nm) emission cross section was measured in the laboratory utilizing a large collision chamber (1.5 m in diameter). Electrons were produced with an electrostatically focusing gun with a large focal length (50 cm). The OI(130.4 nm, 135.6 nm) excitation functions were put on an absolute scale as described in the text, and the OI(135.6 nm)/OI(130.4 nm) ratio was determined for the entire energy range (0–600 eV). The atomic O UV emission cross sections from dissociative excitation of O_2 can be used to model the recent Hubble Space Telescope observations of OI(130.4 nm) and OI(135.6 nm) intensities from Ganymede [*Feldman et al.*, 2000] and Europa [*Hall et al.*, 1995, 1998]. *INDEX TERMS:* 0310 Atmospheric Composition and Structure: Airglow and aurora; 0355 Atmospheric Composition and Structure: Thermosphere—composition and chemistry; 2407 Ionosphere: Auroral ionosphere (2704); 6005 Planetology: Comets and Small Bodies: Atmospheres—composition and chemistry; 6218 Planetology: Solar System Objects: Jovian satellites

Citation: Kanik, I., C. Noren, O. P. Makarov, P. Vattipalle, J. M. Ajello, and D. E. Shemansky, Electron impact dissociative excitation of O_2: 2. Absolute emission cross sections of the OI(130.4 nm) and OI(135.6 nm) lines, *J. Geophys. Res.*, *108*(E11), 5126, doi:10.1029/2000JE001423, 2003.

1. Introduction

[2] Magnetospheric electron populations are maintained in the environment of the outer planets by an unknown process that converts rotational energy into acceleration of newly created ions. A large fraction of those electrons are sufficiently energetic to cause further ionization and to create an ionosphere in those atmospheres. The secondary electrons are especially reactive in collision processes because the excitation cross sections of the atmospheric gases as well as the electron energy distribution produced in the ionosphere attain their peak values at low energies, typically from a few tenths of an eV to ~100 eV. The bright OI(130.4 nm and 135.6 nm) emission lines observed by the Hubble Space Telescope (HST) from Europa, Ganymede, and Io [*Hall et al.*, 1995, 1998; *Feldman et al.*, 2000; *Roesler et al.*, 1999] demonstrate the importance of the electron impact-induced excitation and subsequent fluorescence from atomic and molecular species together with their ions, such as O, S, O_2, H_2O, and SO_2. However, a fundamental limitation in measuring the compositional structure and the energy deposition is set by the accuracy of the emission cross sections used in energy loss codes as well as the identity of the parent oxygen-bearing species, i.e., O, O_2, SO_2, SO, etc., responsible for the observed emissions. The discovery of atmospheric oxygen on a planet or satellite in the solar system containing an oxygen-bearing atmosphere can be obtained from the FUV airglow spectrum.

[3] The atomic oxygen FUV emissions at 135.6 nm and 130.4 nm and the visible emission at 630.0 nm from astronomical sources provide valuable (perhaps unique) information on densities, gas dynamics, etc., of the atmospheres of these satellites of the outer planets. The presence of the spin-forbidden emissions at 135.6 nm or 630.0 nm indicates the existence of a strong electron excitation source as opposed to the solar fluorescence excitation mechanism possible for OI(130.4 nm). For example, in the Jovian system the emissions of OI(135.6 nm) and OI(130.4 nm)

0148-0227/03/2000JE001423

tend to dominate the FUV airglow spectrum on Io [*Ajello et al.*, 1992a, 1992b; *Clarke et al.*, 1994], Europa [*Hall et al.*, 1995, 1998], and Ganymede [*Hall et al.*, 1998; *Feldman et al.*, 2000]. Even on Earth, the intensity of the FUV spectrum contains 90% atomic oxygen emissions [*Torr et al.*, 1995]. Deep aurora on Earth will produce a strong pair of OI(130.4 nm) and OI(135.6 nm) electron-excited aurora from O_2 near the thermopause (L. Paxton and D. Strickland, personal communication, 2001). Midcourse Space Experiment (MSX) spectra have observed dramatic changes in the OI(135.6 nm)/OI(130.4 nm) intensity ratio, depending on the hardness of the primary electrons. For example, the electron impact-induced aurora emission (caused by ~10 keV electrons) from the OI(135.6 nm) feature can become stronger than that of the OI(130.4 nm) feature, as on the satellites of Jupiter.

[4] For the outer planets and their satellites, solar fluorescence as a source of OI(130.4 nm) emission can safely be ruled out based on the weakness of the solar flux at 5 AU and on the fact that the ratio of OI(135.6 nm)/OI(130.4 nm) is found to vary between 1 and 2 [*Hall et al.*, 1995, 1998; *Feldman et al.*, 2000]. On Galilean satellites such as Europa and Ganymede the OI(135.6 nm) emission feature is often found to be the brightest OI emission feature (with the best signal-to-noise ratio) in the HST observational spectra reported by investigators [*Hall et al.*, 1995, 1998; *Feldman et al.*, 2000].

[5] It should be noted here that in some cases a line emission rate can be affected by cascade contributions from the upper states. In case of the OI(130.4 nm) and OI(135.6 nm) emission lines, which result from the transitions $^3P \leftarrow ^{3,5}S$, respectively, cascading from upper states plays an important role in the emission rate. For example, the OI(844.7 nm) and OI(777.4 nm) lines make the largest cascade contributions into the OI(130.4 nm) and OI(135.6 nm) lines, respectively. A detailed discussion on this subject is given by *Kanik et al.* [2000]. Similarly, the trapping of resonance radiation can affect the photon emission rate of certain emission lines. For example, the OI(130.4 nm) resonance line intensity is reduced significantly at high gas pressure regimes due to the self-absorption effect. The background gas pressure must be carefully chosen to ensure optically thin conditions in order to avoid this effect. (For a given resonant transition the operating pressure must result in an optical depth at the line center of >0.1 for the optical path length involved [*Ajello et al.*, 1989].) However, in the case of the OI(135.6 nm) line the self-absorption effect is not important.

[6] It is well known that the OI(135.6 nm) feature arises from a long-lived transition with a lifetime of ~180 μs compared to the prompt radiation from the OI(130.4 nm) feature. The OI(135.6 nm) excitation function was first measured nearly 30 years ago by *Ajello* [1971]. At that time it was assumed that the atomic O dissociation fragments were characterized by a thermal distribution and that the lifetime of the $^5S^o$ state was 590 μs. Ajello estimated the cross section for dissociative excitation to be 1.65×10^{-18} cm^2 at 100 eV. This value was stated to be a lower limit since it was recognized that the O($^5S^o$) atoms from dissociative excitation of O_2 would probably have a nonthermal distribution. *Wells et al.* [1971] tried to improve on the result by using the velocity distribution measured by *Freund* [1971] in a time of flight experiment as a correction to the *Ajello* [1971] result. Freund found that the peak kinetic energy released was 1.2 eV for the O($^5S^o$) metastable fragments. We have verified this peak in the kinetic energy distribution in the companion paper [*Makarov et al.*, 2003] by measuring the Doppler line profile of the OI(135.6 nm) emission feature from dissociative excitation of O_2. *Wells et al.* [1971] found the cross section for dissociative excitation to be 1.1×10^{-17} cm^2 at 100 eV. We can now correct the *Ajello* [1971] calculation at 100 eV for the current shorter lifetime of 180 μs. We find that the corrected result agrees closely with our more accurate measurement of the OI(135.6 nm) emission cross section at 100 eV, described in section 3 and by *Noren et al.* [2001].

[7] In this paper, we present the first new absolute measurement in 30 years of the OI(135.6 nm) excitation function from threshold to 600 eV. We achieve this new measurement by utilizing two state-of-the-art instruments in a two-step procedure. First, the OI(135.6 nm) relative excitation function was measured utilizing the 3 m high-resolution spectrometer described in the companion paper [*Makarov et al.*, 2003] and by *Liu et al.* [1995]. This spectrometer system employs an instrument configuration with a 100-fold increase in the S/N ratio (pulse counting versus analog methods) over that of the instrument described in *Ajello* [1971]. Second, we normalized the OI(135.6 nm) relative excitation cross section at 100 eV to our new measurement of the OI(135.6 nm) absolute cross section at 100 eV, obtained with a new apparatus assembled at the University of Colorado, Boulder, for studying metastable transitions. With this new apparatus we measured the OI(135.6 nm)/OI(130.4 nm) emission cross section ratio at 100 eV. The experiment was conducted in a large vacuum chamber located at the Laboratory for Atmospheric and Space Physics (LASP), University of Colorado. A large experimental vacuum apparatus was required to study the extended glow region of OI(135.6 nm) about an electron beam. The cross section ratio of OI(135.6 nm)/OI(130.4 nm) is determined by measuring the intensity of the prompt radiation from the OI(130.4 nm) emission at the electron beam and comparing it to the extended glow integrated intensity of the OI(135.6 nm) emission. By utilizing the previously measured OI(130.4 nm) cross section at 200 eV from electron impact dissociative excitation of O_2 [*James et al.*, 1988], the absolute emission cross section for the OI(135.6 nm) feature is determined to be 6.4×10^{-18} cm^2. The emission cross sections for the OI(130.4 nm) and OI(135.6 nm) features are given in analytic form for inclusion in electron energy loss codes in O_2 gas.

[8] A calculation of the OI(135.6 nm)/OI(130.4 nm) emission rate is presented for monoenergetic and Maxwellian distributions. The results are compared to the HST observations of OI(135.6 nm)/OI(130.4 nm) to ascertain electron temperatures and verify the $e + O_2$ dissociative excitation process as the source of the atomic oxygen emissions. In addition, we also obtained the OI(115.2 nm) absolute optical excitation function in the 0–600 eV electron impact range for the first time from dissociative excitation of O_2.

2. Experimental Apparatus

[9] The experiment requires passing an electron beam through a static oxygen gas and measuring the glow

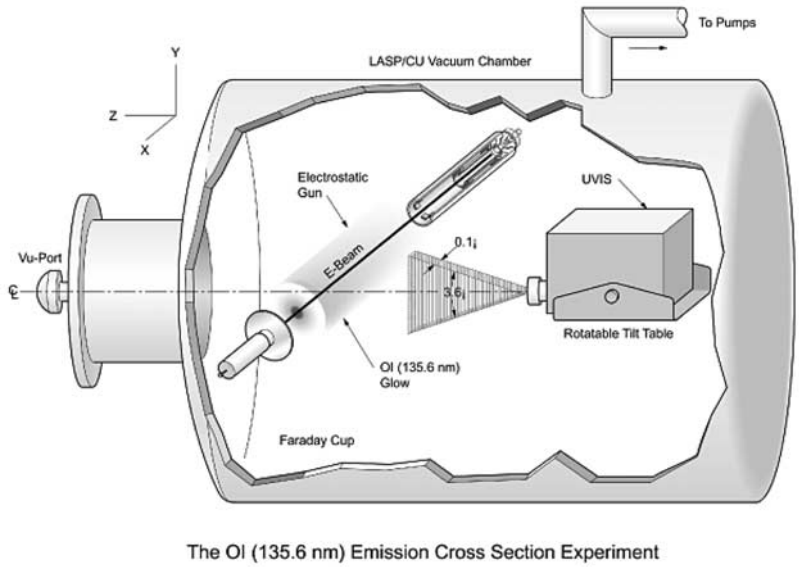

Figure 1. The 1.5 m Laboratory for Atmospheric and Space Physics (LASP), University of Colorado, vacuum chamber with the electrostatic electron gun and the Ultraviolet Imaging Spectrograph (UVIS).

pattern produced around the electron beam. Ideally, an infinitely long electron beam will produce a cylindrically uniform glow region, where the emission and excitation rates per unit length of the beam are equal. We can approximate this condition by making the chamber and the electron beam as long as possible. The experimental apparatus at the University of Colorado consisted of an electrostatic electron gun, a Faraday cup, two pairs of Helmholtz coils, a large (1.5 m diameter $\times$ 2.35 m length) vacuum chamber with a movable detector platform, a gas source, and the Cassini Ultraviolet Imaging Spectrograph (UVIS) FUV flight-spare engineering detector mounted on a programmable tilt-table platform with *xyz* translation and/or *x* axis rotation. The Faraday cup system on a smaller scale has been shown elsewhere [*Liu et al.*, 1995]. The vacuum chamber was pumped by a cryopump procured from ADP Cryogenics and obtained a base pressure of 6.6×10^{-7} torr, as monitored by an ionization gauge. The instrument is shown schematically in Figure 1.

[10] The electron gun was constructed from the two-cylinder (ratio of diameters is 2) lens design of *Harting and Read* [1976] such that the lens voltages can be set to establish a 50 cm focal length with a 20 μA beam current at 30 eV. The long trajectory of the electron beam required the use of two pairs of Helmholtz coils to negate the effects of the Earth's magnetic field components that were perpendicular to the electron beam. In the present setup an electron beam with an energy of 100 eV can be deflected by the Earth's magnetic field (of the order of 500 mG) $\sim$15 cm from its intended path. To help focus and steer the electron beam, a large electrical shield ($\sim$60 cm in diameter) was mounted as the front element of the Faraday cup. The shield was placed in series with an electrometer and was used to collect any stray electrons. This aided in the focusing of the electron beam by the lenses as well as in the beam alignment with the Helmholtz coils. The electron beam current was typically 90 μA with only 100 nA measured on the outer shield, indicating that the beam was well-focused. This was checked visually by passing the electron beam through pure nitrogen and observing with the naked eye through a Plexiglas port the visible glow produced along the electron beam path (see Figure 1).

[11] The size and shape of the observed glow region depends upon two factors: the lifetime of the transition and the velocity distribution of the emitting atoms. The OI($^5S^o$) state has a long lifetime (180 μs) since there is no dipole-allowed transition available to it, and the excited oxygen atoms produced by dissociative excitation of O_2 have a nonthermal velocity distribution. *Makarov et al.* [2003] have recently measured the kinetic energy distributions of these atomic oxygen fragments and found that they peak at $\sim$1.3 eV, which corresponds to a glow region $\sim$0.5 m in radius, and that they have a mean kinetic energy of 2.4 eV. The glow volume emission rate has been modeled using the technique of *Ajello* [1970] (briefly described in section 3) and shows the glow intensity falling off faster than $1/r$, where r is distance from the electron beam. We present in Figure 2 the expected volume emission rate for three cases: (1) the important case of 180 μs lifetime and 2.4 eV mean kinetic energy (solid line); (2) the glow region predicted by *Ajello* [1971] (dotted line); and (3) the glow region predicted by *Wells et al.* [1971] (dashed line). From Figure 2 we see that the volume emission rate falls by 2 orders of magnitude at 0.5 m, while the integrated column emission intensity as a function of minimum ray height from the beam will fall less rapidly with distance [*Ajello*, 1970].

[12] It should be pointed out here that the angular distribution of the atomic fragments after the dissociation is important and should be taken into account. Direct dissociation of a molecule occurs on a timescale which is fast compared to its rotation. The dissociation fragments tend to fly apart in the direction of vibration. Thus if the molecule has a preferred direction (relative to incident

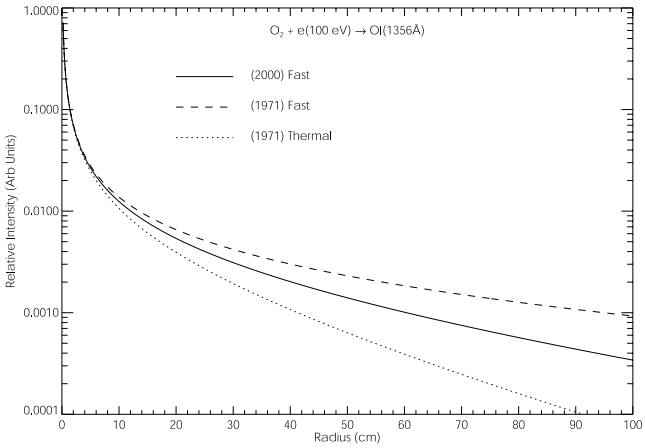

Figure 2. A model of the OI(135.6 nm) glow region volume emission rate about the electron beam. The solid line shows the present result. (A 180 μs lifetime is used for the $^3P \leftarrow {}^5S$ transition at 135.6 nm, and a 2.4 eV mean kinetic energy is used for the OI atoms.) The dotted line shows the glow region predicted by *Ajello* [1971], and the dashed line shows the glow region predicted by *Wells et al.* [1971].

electron beam) for the initial excitation to occur, an anisotropic distribution of the fragments can result. This has been analyzed by *Dunn* [1962] and *Zare* [1967], and they found that this phenomenon is only significant at very low (near threshold) energies and only for simple molecules like H_2. At higher impact energies the angular distribution quickly becomes isotropic (see *Misakian et al.* [1975] for work on CO_2; *Cosby* [1993a, 1993b, 1993c] for work on O_2, N_2, and CO; and *LeClair* [1993] for work on O_2). In the present investigation the isotropic distribution of the dissociation fragments is assumed for the reasons given above.

[13] The 135.6 nm radiation was detected using the Cassini UVIS FUV flight-spare engineering detector, which is a two-dimensional array detector (64 [spatial] × 1024 [wavelength] pixels) with a CsI photocathode that is sensitive over the wavelength range from 110.0 to 190.0 nm. A detailed description of the UVIS can be found in the work of *McClintock et al.* [1993]. The 64 pixel spatial pixels are oriented perpendicular to the electron beam and define a field of view (FOV) of 3.6°. The slit width is 75 μ wide, which yields an effective FOV in the plane of dispersion of 0.1°. In the plane of dispersion the full width at half maximum (FWHM) of the UVIS is 6 pixels, or 0.4 nm. The operation of the UVIS allows for the entire spectrum to be collected simultaneously, and thus the 130.4 nm and 135.6 nm emission lines are always imaged concurrently. The lifetime of the OI(130.4 nm) emitting state is 1.6 ns, and thus its glow region is roughly the shape of the electron beam since it does not have time to drift before radiating. The electron beam was estimated to be ∼5 mm in diameter at the center of the viewing region, where the Cassini UVIS optic axis intersects the electron beam. Since the UVIS telescope with an off-axis parabolic mirror has a focus built for infinity at the entrance slit focal plane, the OI(130.4 nm) image appeared on ∼25 pixels FWHM in the spatial direction. A properly focused electron beam

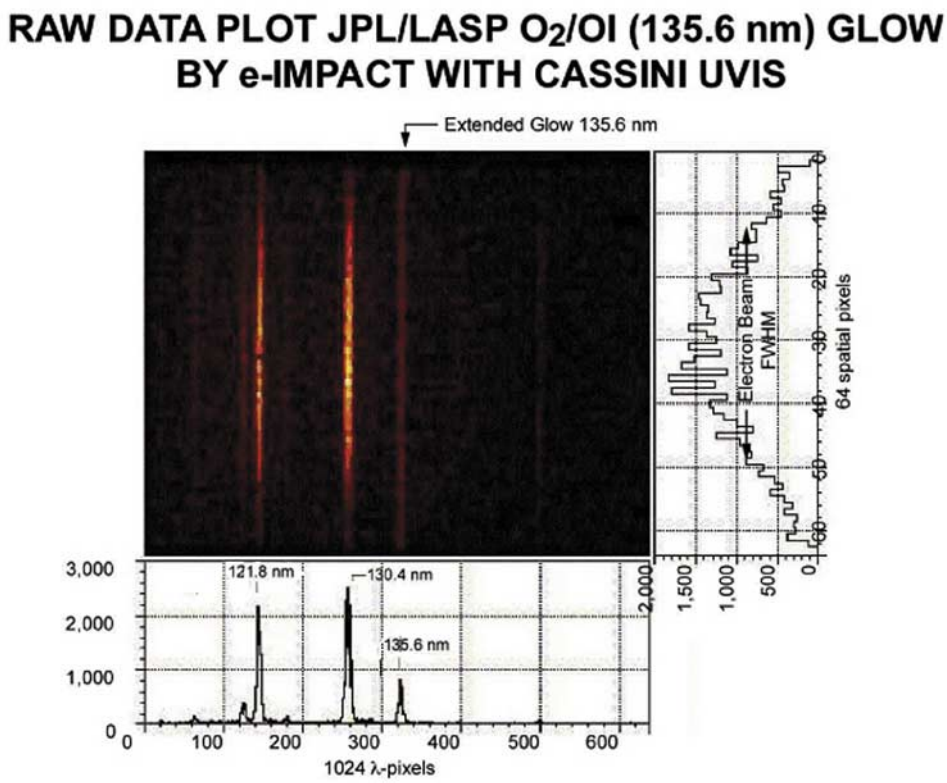

Figure 3. The extended glow region intensity of OI(135.6 nm) as measured by the UVIS 1024 × 64 Codacon array.

image of the OI(130.4 nm) emission with a corrector lens should only appear on five or six pixels. The UVIS image of the glow region for a zero degree tilt angle is shown in Figure 3. This defocusing aberration did not affect the measurement of the total counts of OI(130.4 nm) or OI(135.6 nm) because of the co-adding of the 64 spatial pixels. Additionally, the change with intensity of the long-lived OI($^5S^o$) emission with distance from the electron beam is <10% over the spatial dimension of the detector for all 64 adjacent pixels defining 64 lines of sight of the UVIS at OI(135.6 nm). Thus the UVIS detector could accurately map the OI(135.6 nm) emission with respect to the tilt angle of the UVIS. As shown in Figure 3, the OI(135.6 nm) feature is spread with roughly equal intensity on all pixels.

[14] When the UVIS's optic axis was directed at the midpoint of the electron beam, not all of the excited OI($^5S^o$) atoms remained in the FOV of the detector before emitting 135.6 nm photons. This is due to the long lifetime of the OI($^5S^o$) state, which allowed a significant portion of these excited atoms to drift out of the 3.6° FOV of the detector before radiating. To measure all the OI(135.6 nm) photons, we made use of the moveable platform that had two linear degrees of freedom, horizontal (x axis) and vertical (y axis) motion, and two angular degrees of freedom, tilt (rotation about the x axis) and azimuth (rotation about the y axis) (see Figure 1). The z axis was defined as the optic axis of the detector when it is closest to and pointed at the midpoint of the electron beam. The detector was mounted on this platform to scan a larger portion of the glow region and thus allowed us to accurately measure the glow profile and the total line of sight-emitted line intensity with respect to angle. In particular, the platform could be rotated about the x axis, which is parallel to the electron beam, so that the detector's line of sight ranged from 35 cm below the electron beam to 15 cm above it. Using this tilt angle range and the glow model discussed in section 3, we determined that the UVIS was able to measure only ~48% of the emitted OI(135.6 nm) photons.

[15] To verify that we had indeed produced symmetric glow in the midregion, the glow in the midregion was mapped out, both on-axis and off-axis, to ensure the emission intensity did not vary as a function of position along the electron beam axis. No variation was observed in this region. This is not problem for the 130.4 nm radiation from the OI($^3S^o$) state due to the short lifetime of the $^3S^o$ state (1.6 ns).

3. Experimental Results

[16] Figure 4 shows the OI(130.4 nm) and OI(135.6 nm) calibrated emission intensities resulting from a radiative decay of the excited OI($^3S^o$ and $^5S^o$) states by electron impact-induced dissociative excitation of O_2 as a function of angular displacement. The calibration sensitivity of the UVIS at 130.4 nm and 135.6 nm was measured to be the same [*McClintock et al.*, 1993]. The spectrum was obtained at a gas temperature of nearly 300 K and at a spectral resolution of 0.5 nm FWHM. A 100 eV electron beam was passed through a static oxygen gas (O_2) and the glow pattern produced around the electron beam. The

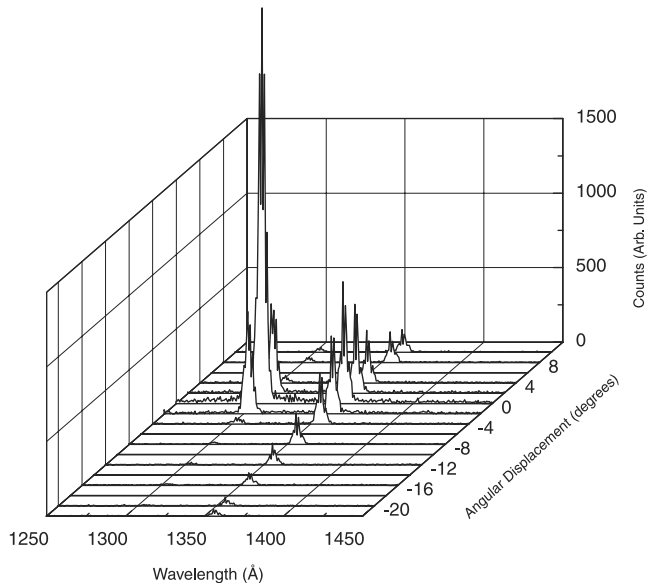

Figure 4. Variation of the OI(135.6 nm) line intensity with tilt angle.

axially symmetric glow of emitted photons at 130.4 nm and 135.6 nm produced within O_2 were detected at 90° with respect to the boresight of the Cassini UVIS.

[17] As mentioned earlier, the trapping of resonance radiation can reduce the photon emission rate significantly at high gas pressure. Since 135.6 nm is not a dipole-allowed OI transition, radiation trapping is not a concern. However, 130.4 nm can be resonantly absorbed by OI, and thus the amount of atomic oxygen present in the chamber must be minimized. Since the production of OI is due to the electron impact-induced dissociative excitation of O_2, the amount of OI in field of view was negligible. The gas (O_2) pressure range (7×10^{-6} torr) was maintained in the chamber during the present measurements. No correction due to the polarization of radiation was required since the radiation is unpolarized because it is emitted from an "S state" for both transitions. The lifetime of the $^5S^o$ state is relatively long (~180 μs [*Biemont and Zeippen*, 1992]), and atoms can experience a drift of the order of 0.5 m before they undergo radiative decay. As seen from Figure 4, the integrated emission intensity of the OI(130.4 nm) multiplet drops off very rapidly toward zero. However, as expected owing to its long lifetime, the OI(135.6 nm) multiplet line of sight-integrated emission intensity gradually decreases as the line of sight of the detector is moved above (below) the electron beam.

[18] Figure 5 shows the integrated emission intensities for the OI(135.6 nm) and OI(130.4 nm) features as a function of minimum ray height from the electron beam. The two sets of data were curve-fitted with a cubic spline function, and the area under each curve was integrated with respect to angle to obtain the total emission intensity for the features being studied. The total estimated signal in counts s^{-1} from OI(135.6 nm) is proportional to the integral of the line of sight-integrated emission intensity with respect to all tilt angles. The line of sight OI(135.6 nm) intensity I (photons cm^{-2} s^{-1}) can be written as the integral of the

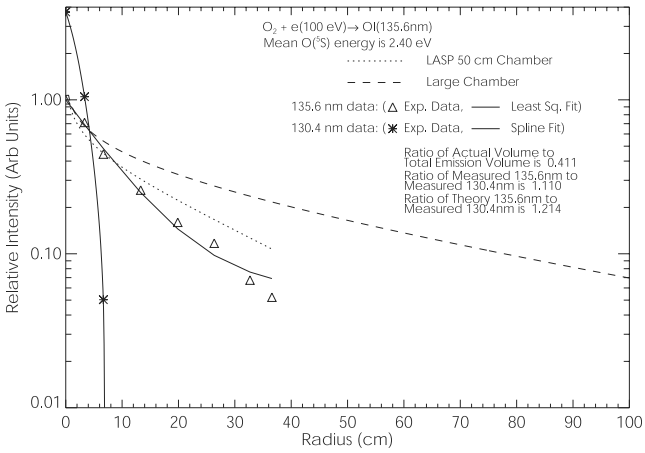

Figure 5. The measured line of sight-integrated signal intensities of OI(130.4 nm) (asterisks) and OI(135.6 nm) (triangles) with minimum ray height. The data points are joined by a spline function. Also shown are models for the integrated intensities for the following cases: the actual LASP chamber where some of the excited OI(^5S) atoms collide with the wall (dotted line) and a very large chamber where none of the excited OI(^5S) atoms collide with the wall (dashed line).

volume emission rate I_v (photons cm^{-3} s^{-1}) along the variable of the line of sight p. I is given by

$$I = \int I_v(p)dp. \tag{1}$$

The total signal in counts s^{-1} from the chamber in terms of the minimum ray height a from the electron beam is

$$\mathrm{Sig}(135.6\ \mathrm{nm}) = \varepsilon_{1356} A_{\mathrm{mir}} \int (I(a)/4\pi) d\Omega_{\mathrm{FOV}}(a), \tag{2}$$

where A_{mir} is the area of the telescope mirror, $d\Omega_{\mathrm{FOV}}$ is the full field of the Cassini detector (3.6° × 0.1°), and ε_{1356} is the efficiency of the optical system in counts photon^{-1} at 135.6 nm. The total signal in equation (2) is over the solid angle wedge (0.1° in width), with a vertical extent defined by all measured tilt angles, which is to 22° in our experiment. At 22° the minimum ray height is 37 cm.

[19] The experimental ratio, OI(135.6 nm)/OI(130.4 nm), based on the observed data points shown in Figure 4 was found to be 1.11. However, on the basis of the equality of the emission per unit length with the excitation per unit length, the total measured OI(135.6 nm) signal in Figure 5 accounted only for 48.5% of the total emission coming from this feature. As explained in this section, when corrected for the total emission for a very large chamber, the integrated emission intensity (with respect to angle) ratio of the OI(135.6 nm) to OI(130.4 nm) was determined to be 2.29 at 100 eV. In Figure 5 we show two models of the integrated emission intensity as a function of the minimum ray height. The dotted line is the model of the measurement with the finite size chamber that always cuts off some of the line of sight-emitted intensity. The dashed line is the model for a very large chamber (∼8 m in diameter), where none of the excited O($^5S^o$) atoms collide with the wall. The comparison of the two models shows that some of the excited atoms collide with the wall before they radiate at all tilt angles. The ratio of the measured OI(135.6 nm) emission intensity to that of OI(130.4 nm) is found to be 1.11. The same ratio under the model profile is determined to be 1.21, which is in excellent agreement with the measured ratio.

[20] Figure 6 gives the fraction of the excited atoms detected for all lines of sight as a function of radius of the chamber. As seen from Figure 6, at the zero degree tilt angle we observed 90% of the radiation. At the final tilt angle of 22°, however, we observed only ∼53% of the radiation. In other words, the fraction of atoms remaining in the chamber with high velocity increased with tilt angle or minimum ray height. Summed over all tilt angles of the LASP chamber, we observed 48.5% of the total emitted radiation. The model accurately depicts the glow profile.

[21] The integrated emission intensity for the OI(130.4 nm) feature from electron impact dissociative excitation of O_2 at 100 eV was put on an absolute scale, utilizing both the previously measured OI(130.4 nm) cross section at 200 eV [*James et al.*, 1988] and the new excitation function measurement of the OI(130.4 nm), as discussed in section 4. The cross section of OI(130.4 nm) at 100 eV is determined to be 2.83 × 10^{-18} cm^2 at 100 eV. From the ratio of the integrated intensities of the OI(135.6 nm) and OI(130.4 nm) features and from the absolute emission cross section for the OI(130.4 nm) emission feature from electron impact dissociative excitation of O_2 at 100 eV, the absolute emission cross section for the OI(135.6 nm) feature was determined to be 6.4 × 10^{-18} cm^2.

4. Discussion

4.1. Optical Excitation Function Measurements

[22] Electron impact-induced emission cross sections for optically allowed transitions at 115.2 nm and 130.4 nm and for an optically forbidden transition at 135.6 nm were obtained by the Jet Propulsion Laboratory 3 m high-resolution spectrometer over the electron impact energy range 0–600 eV. The 3 m high-resolution spectrometer used for the measurements is described in the companion paper

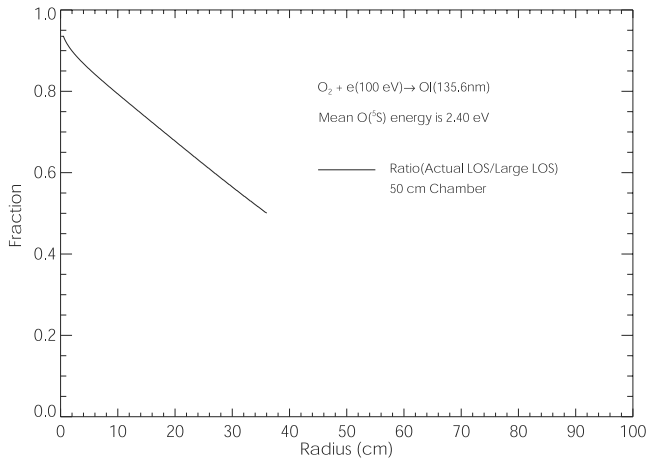

Figure 6. Fraction of the excited OI(^5S) atoms observed for all lines of sight as a function of the radius of the chamber for the present measurement (solid line). A mean kinetic energy of 2.4 eV is used.

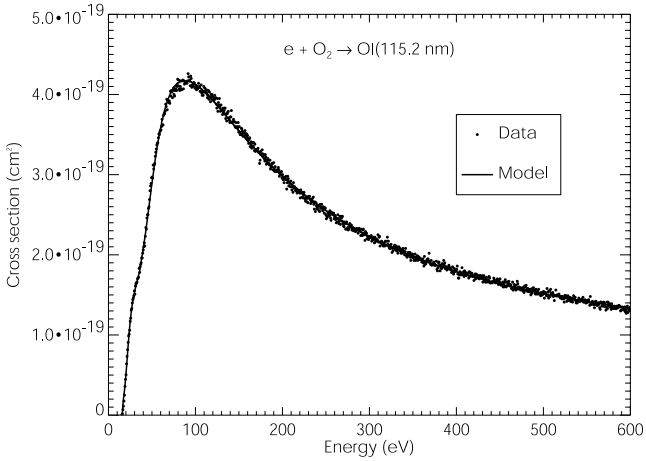

Figure 7. The measured OI(115.2 nm) excitation function with a curve fit function model.

[*Makarov et al.*, 2003] for the 0–50 eV excitation functions of the same multiplets. The excitation function data and modified Born approximation model fit for the transitions at 115.2, 130.4, and 135.6 nm are shown in Figures 7, 8, and 9, respectively. The excitation functions for optically allowed transitions at 115.2 nm and 130.4 nm were put on an absolute scale by normalizing them to the cross section values of 3×10^{-19} cm^2 [*Ajello and Franklin*, 1985] and 2.1×10^{-18} cm^2 [*James et al.*, 1988] at 200 eV, respectively. For the optically forbidden transition at 135.6 nm the measured cross section value of 6.4×10^{-18} cm^2 at 100 eV was used to put the excitation function on an absolute scale.

[23] The individual data sets were fitted within experimental error using the following analytical form for collision strength given by *Shemansky et al.* [1985a, 1985b]

$$\Omega(x) = C_0(1 - 1/X)X^{-2} + \sum_{k=1}^{4} C_k(X-1)\exp(-kC_8X) + C_5 + C_6/X + C_7\ln(X), \quad (3)$$

where $\Omega(x)$ is the collision strength, X is the electron impact energy in threshold units, and C_k are constants of the function $\Omega(x)$.

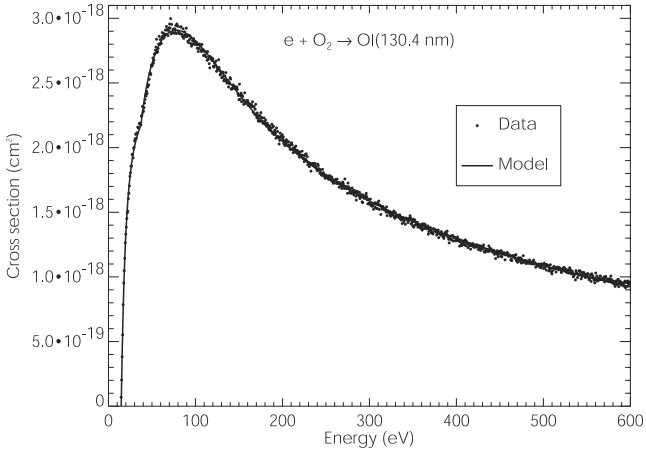

Figure 8. Same as Figure 7, but for OI(130.4 nm).

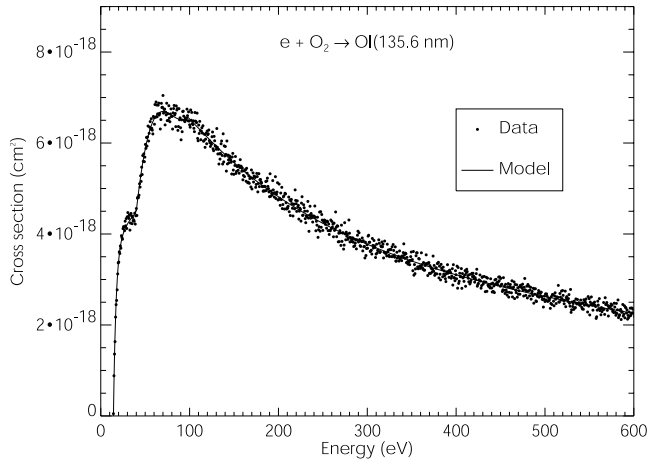

Figure 9. Same as Figure 7, but for OI(135.6 nm).

[24] We list in Table 1 the constants of equation (3). The excitation cross section is the given by the equation

$$Q(X) = \Omega(X)(EX)^{-1}, \quad (4)$$

where $Q(X)$ is the cross section in atomic units and E is the transition energy in Rydberg units. We list in Table 2 the present cross section data for the OI(130.4 nm) feature as a function of energy. Also included in Table 2 are the results from four previous cross section measurements of *Ajello* [1971], *Lawrence* [1970], *Aarts and De Heer* [1971], and *Zipf* [1986]. A comparison of the previous measurements with the present results is given in Figure 10. As seen from Figure 10, our model fit to the present measurement is in good agreement with all the previous measurements.

[25] An energy-dependent correction factor (hereinafter referred to as the field of view factor) was applied to the excitation function measurements shown in Figure 9 for OI(135.6 nm). The field of view factor is described by P. Vatti Palle et al. (The high-resolution far ultraviolet spectrum of electron-excited SO_2, submitted to *Journal of Geophysical Research*, 2003). Each dissociation process produces its own characteristic velocity distribution. The fractional contribution of each of these processes leads to an energy-dependent field of view factor.

[26] We list in Table 3 the cross section data as a function of energy for the OI(115.2 nm and 135.6 nm) features. The OI(115.2 nm) excitation function has not been previously reported. However, the cross section for the OI(115.2 nm) feature has been measured at 200 eV by *Morgan and Mentall* [1983] and can be revised downward to 5.1×10^{-19} cm^2 by the presently accepted NI 120.0 nm 200 eV dissociative excitation cross section of N_2 [*James et al.*, 1990]. *Ajello and Franklin* [1985] reported the value of the OI(115.2 nm) cross section as 4.1×10^{-19} cm^2 at 100 eV and 3.0×10^{-19} cm^2 at 200 eV. The latter cross section is used to normalize the present OI(115.2 nm) excitation function.

[27] The OI(135.6 nm) relative excitation function, however, was measured by *Ajello* [1971]. *Wells et al.* [1971] later tried to improve on the *Ajello et al.* [1971] result by using the velocity distribution measured by *Freund* [1971]. However, the *Wells et al.* [1971] cross section for the OI(135.6 nm) emission feature is ~60%

Table 1. Collision Strength Analytical Coefficients for $e + O_2 \rightarrow$ OI(130.4, 135.6, and 115.2 nm)[a]

	$e + O_2 \rightarrow$ OI(130.4 nm)		$e + O_2 \rightarrow$ OI(135.6 nm)		$e + O_2 \rightarrow$ OI(115.2 nm)	
Process	E_{ij} = 14.67 (93%)	E_{ij} = 40.20 (7%)	E_{ij} = 14.26 (95%)	E_{ij} = 37.50 (5%)	E_{ij} = 15.90 (80%)	E_{ij} = 36.00 (20%)
C_0	0.0000000E+00	0.0000000E+00	0.48000650E−01	0.25263500E−02	0.00000000E+00	0.00000000E+00
C_1	−0.18059670E−01	−0.13593300E−02	−0.77856300E−01	−0.40977000E−02	−0.57473600E−01	−0.14368400E−01
C_2	0.00000000E+00	0.00000000E+00	−0.39284400E−01	−0.20676000E−02	0.00000000E+00	0.00000000E+00
C_3	0.00000000E+00	0.00000000E+00	0.00000000E+00	0.00000000E+00	0.00000000E+00	0.00000000E+00
C_4	−0.27565200E+00	−0.20748000E−01	−0.53260800E+00	0.28032000E−01	0.97632000E−01	0.24408000E−01
C_5	0.18301470E+00	0.13775300E−01	0.47435400E+00	−0.24966000E−01	0.19560000E−01	0.48900000E−02
C_6	−0.18301470E+00	−0.13775300E−01	−0.47435400E+00	−0.24966000E−01	−0.19560000E−01	−0.48900000E−02
C_7	0.75495540E−01	0.56824600E-02	0.16287750E+00	0.85725000E−02	0.97512000E−02	0.24378000E−02
C_8	0.15136000E+00	0.15136000E+00	0.16596000E+00	0.16596000E+00	0.74131000E+00	0.74131000E+00

[a]E_{ij} is appearance potential in units of eV. To obtain cross section Q, use equation (4). $Q \times$ 8.8E−17 gives cross sections in units of cm^2. Total cross section, Q_{total}, can be obtained from $Q_{total} = Q(E_1) + Q(E_2)$ (i.e., the cross sections must be on absolute energy scale for summation).

Table 2. Absolute Cross Sections of Electron Impact Dissociation of O_2 for OI($3s^3S^o \rightarrow 2p^3P$; λ1304 Å)[a]

Energy, eV	This Work[b]	*Ajello* [1971][c]	*Lawrence* [1970][d]	*Aarts and De Heer* [1971][e]	*Zipf* [1986][f]
14		0.117			
14.8	0.0371				
16	0.507	0.557			
18	1.03	0.830			
20	1.37	1.05			0.758
25	1.84	1.36	1.31		1.49
30	2.06	1.55	1.74		1.85
35	2.19	1.71	2.00		2.13
40	2.37	1.87	2.21		2.29
45	2.58	1.98	2.39		2.57
50	2.72	2.06	2.54		2.80
60	2.89	2.18	2.81		3.07
70	2.97	2.26	2.97		3.10
80	2.98	2.32	3.03		3.11
90	2.95	2.35	3.02		3.11
100	2.90	2.37	2.95	2.66	3.07
125	2.69	2.36	2.73		2.77
150	2.47	2.30	2.47	2.29	2.51
175	2.27	2.20	2.29		2.26
200	2.10	2.10	2.10	2.10	2.10
225	1.95	2.01	1.96		1.96
250	1.83	1.89	1.84		1.85
275	1.72	1.78	1.74		1.76
300	1.63	1.68	1.64	1.58	1.66
400	1.33		1.39	1.36	
500	1.12		1.22	1.16	
600	0.947		1.09	1.02	
700			0.997		
800			0.918	0.845	
900			0.856		
1000			0.792	0.727	
1500				0.521	
2000				0.434	
3000				0.309	
4000				0.242	
5000				0.205	

[a]Electron impact dissociations are in units of 10^{-18} cm^2.

[b]Results of this work were put on an absolute scale using the cross section value 2.10 × 10^{-18} cm^2 of *James et al.* [1988] at 200 eV.

[c]The cross section of *Ajello* [1971] was renormalized to fit the cross section value 2.10 × 10^{-18} cm^2 of *James et al.* [1988] at 200 eV.

[d]The cross section of *Lawrence* [1970] was renormalized to fit the cross section value 2.10 × 10^{-18} cm^2 of *James et al.* [1988] at 200 eV.

[e]The cross section of *Aarts and De Heer* [1971] was renormalized to fit the cross section value 2.10 × 10^{-18} cm^2 of *James et al.* [1988] at 200 eV.

[f]*Zipf* [1986] used older results from the work of *Mumma and Zipf* [1971] but renormalized them to reflect the then new value of the Ly α cross section 7.5 × 10^{-18} cm^2 at 100 eV. We used the most recent value of the Ly α cross section of *Pang et al.* [1987] (7.29 × 10^{-18} cm^2) at 100 eV to renormalize the cross section of *Zipf* [1986]. The fact that the new value of Zipf at 200 eV is also 2.10 × 10^{-18} cm^2 is purely coincidental.

larger than our present value at 100 eV. *Itikawa et al.* [1989] has reviewed the published set of O_2 dissociation cross sections. His Table 7.1 includes a "preliminary" measurement by *Zipf* [1986] of the OI(λ1356 Å) emission cross section of 6.9 × 10^{-18} cm^2 at 100 eV. This measurement is within the error bars of the present result. *Itikawa et al.*'s [1989] emission ratio for OI(135.6 nm)/OI(130.4 nm) at 100 eV is 2.2, and this ratio is also in excellent agreement with our present result of 2.3. *Schulman et al.* [1985] has measured the important set of Rydberg series transitions that cascade to O($3s^5S^o$) from the np ^5P series. The strongest cascade multiplet ($3p \rightarrow 3s$) is OI(777.4 nm) with a cross section of 4.3 ± 0.6 × 10^{-18} cm^2 at 100 eV. This result was verified by *Erdman and Zipf* [1988], who found a cross section of 4.8 × 10^{-18} cm^2 at 100 eV. The next strongest multiplet is $4p^5P$ at 394.7 nm. Taken with the results presented here, the cascade emission cross section is near 5 × 10^{-18} cm^2 at 100 eV. The direct excitation cross section of OI(135.6 nm) must be <1.5 × 10^{-18} cm^2 at 100 eV.

[28] The root-sum-square uncertainties associated with the absolute cross sections are estimated as follows: There is an uncertainty of 3% in the signal statistics, an uncertainty of 22% in the OI(115.2 nm, 130.4 nm, and 135.6 nm) cross sections (see *Ajello and Franklin* [1985] and *James et al.* [1988] for details) from the absolute cross section of OI(130.4 nm) that we used to put the present measurements on an absolute scale, and an uncertainty of 5% from the

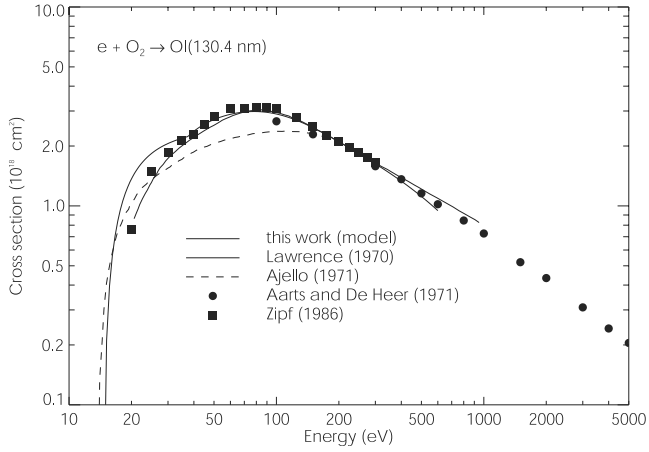

Figure 10. Model of the OI(130.4 nm) excitation function compared to previous results.

fitting procedure. Thus the overall error (square root of the sum of the squares of the contributing errors) in the present measurements is estimated to be ~23%.

4.2. Ratio of the OI(135.6 nm)/OI(130.4 nm) Cross Sections

[29] We obtain the ratio of absolute emission cross sections, σ(135.6 nm)/σ(130.4 nm), for monoenergetic electrons from the data and models of Figures 8 and 9. This monoenergetic emission cross section ratio is shown in Figure 11 as a solid line ("direct ratio") for the electron impact energy range 14–600 eV. We also calculated the ratio of the electron impact emission rate coefficients R (photons s^{-1} molecule^{-1}) for unit electron flux, denoted as R(135.6 nm)/R(130.4 nm), for a Maxwellian electron distribution flux with temperature T_e in the range 5–500 eV. Emission rate coefficients were calculated by integrating with respect to energy the product of the emission cross section for 135.6 nm and 130.4 nm times unit Maxwellian electron energy flux. This ratio is shown in Figure 11 as a dashed line. The emission ratio R(135.6 nm)/R(130.4 nm) varies from ~2.5–3 for cold electrons with T_e = 5 eV to ~2–2.5 for hot electrons with T_e > 40 eV. *Hall et al.* [1995, 1998] reported that the ratio of the integrated brightness for these two multiplets obtained by the HST observations of Europa is highly variable, with intensity ratios between 1.3 ± 0.8 and 2.2 ± 1.4. Similarly, from observation the intensity ratio for Ganymede is found to be in the range 1.2 ± 0.3–3.2 ± 1.6. The astronomical ratios reported by *Hall et al.* [1998] and *Feldman et al.* [2000] are also shown in Figure 11. There are no estimates of the electron temperature near Ganymede. *Sittler and Strobel* [1987] report an electron temperature of at least 20 eV at an L shell of 13. Our findings, based on the calculated Maxwellian-averaged cross section ratios, support a predominant cold electron distribution of ~30 eV in the neighborhood of Ganymede. However, our laboratory-based cross section ratio does not support the Europa brightness observations for any energy. Voyager I observed near Europa a two-temperature distribution of electrons, with cold electrons in the range T_e = 15–25 eV and hot electrons with T_e ~ 250 eV [*Sittler and Strobel*, 1987; *Bagenal*, 1994]. It is plausible that atomic O needs to be added to the atmospheric distribution structure on both Europa and Ganymede to explain the HST results in terms of the intensity ratios. This added result compares favorably with the *Feldman et al.* [2000] analysis using slightly different cross sections.

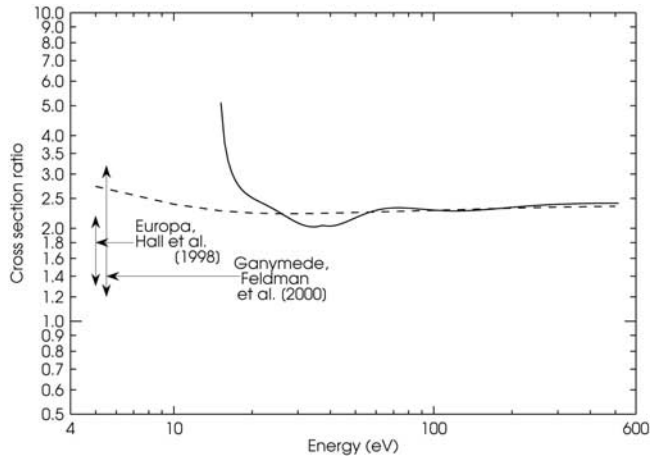

Figure 11. Ratio of the OI(135.6 nm)/OI(130.4 nm) emission cross section as a function of energy for a monoenergetic electron flux (solid line) and a Maxwellian electron flux (dashed line).

Table 3. Absolute Cross Sections of Electron Impact Dissociation of O_2 for OI($3s^5S^o \rightarrow 2p^3P$; λ1356 Å) and for OI($3s^1D^o \rightarrow 2p^1D$; λ1152 Å)[a]

Energy, eV	This Work (1356 Å)[b]	*Ajello* [1971] (1356 Å)[c]	This Work (1152 Å)[d]
14.3	0.0003		
14.7		0.116	
16	1.68	2.19	0.00219
18	2.73	3.27	0.0273
20	3.37	3.77	0.0496
25	4.11	4.68	0.117
30	4.18	5.16	0.154
35	4.32	5.47	0.176
40	4.72	5.69	0.209
45	5.24	5.83	0.247
50	5.74	5.96	0.289
60	6.45	6.11	0.359
70	6.74	6.22	0.398
80	6.76	6.33	0.414
90	6.65	6.38	0.417
100	6.40	6.40	0.413
125	5.98	6.36	0.386
150	5.52	6.22	0.355
175	5.13	6.05	0.324
200	4.79	5.83	0.298
225	4.49	5.63	0.275
250	4.23	5.41	0.255
275	4.00	5.23	0.238
300	3.79	5.05	0.223
400	3.13		0.179
500	2.62		0.152
600	2.21		0.133

[a]Electron impact dissociations are in units of 10^{-18} cm^2.

[b]Results of this work were put on an absolute scale using the cross section value 2.10 × 10^{-18} cm^2 of *James et al.* [1988] at 200 eV for OI($3s^3S^o \rightarrow 2p^3P$; λ1304 Å) and for the ratio of OI(1356 Å)/OI(1304 Å) = 2.29.

[c]The cross section of *Ajello* [1971] was renormalized to fit the cross section value 6.4 0 × 10^{-18} cm^2 at 100 eV of this work.

[d]Results of this work were put on an absolute scale using the cross section value 3.00 × 10^{-19} cm^2 of *Ajello and Franklin* [1985] at 200 eV.

[30] **Acknowledgments.** The research described was carried out at the Jet Propulsion Laboratory, California Institute of Technology, and at the Laboratory for Atmospheric and Space Physics, University of Colorado. This work was supported by the NASA Planetary Atmospheres Program Office. We thank W. McClintock, V. Drake, E. Devito, and K. Filsinger at LASP for their efforts in maintaining the Moby Tank vacuum system. We also thank P. Hardy and M. Hetzel from Alliance Space Systems, Inc. for their expertise in designing and manufacturing the electron gun-Faraday cup system. O. Makarov and P. Vatti Palle acknowledge support by the National Research Council Resident Research Associate Program. We thank A. Chutjian for discussions about the electrostatic electron gun design.

References

Aarts, J. F. M., and F. J. De Heer, Emission cross sections for OI and OII multiplet radiation produced by electron impact on O_2, *Physica*, *56*, 294–296, 1971.

Ajello, J. M., Emission cross sections of N_2 in the vacuum ultraviolet by electron impact, *J. Chem. Phys.*, *53*, 1156–1165, 1970.

Ajello, J. M., Dissociative excitation of O_2 in the vacuum ultraviolet by electron impact, *J. Chem. Phys.*, *55*, 3156–3157, 1971.

Ajello, J. M., and B. Franklin, A study of the extreme ultraviolet spectrum of O_2 by electron impact, *J. Chem. Phys.*, *82*, 2519–2528, 1985.

Ajello, J. M., G. K. James, I. Kanik, and B. O. Franklin, Medium-resolution studies of extreme ultraviolet emission from N_2 by electron impact: Vibrational perturbations and cross sections of the $c'_4\,^1\Sigma_u^+$ and $b'\,^1\Sigma_u^+$ states, *Phys. Rev. A Gen. Phys.*, *40*, 3524–3556, 1989.

Ajello, J. M., G. K. James, I. Kanik, and B. O. Franklin, The complete UV spectrum of SO_2 by electron impact: 1. The vacuum ultraviolet spectrum, *J. Geophys. Res.*, *97*, 10,473–10,500, 1992a.

Ajello, J. M., G. K. James, and I. Kanik, The complete UV spectrum of SO_2 by electron impact: 2. The middle ultraviolet spectrum, *J. Geophys. Res.*, *97*, 10,501–10,512, 1992b.

Bagenal, F., Empirical models of the Io plasma torus: Voyager measurements, *J. Geophys. Res.*, *99*, 11,043–11,062, 1994.

Biemont, E., and C. J. Zeippen, Electric-dipole trasitions in atomic oxygen and the lifetimes of the 2*P*3(4*S*0)3*S*5*S*0 and *S*-3 (0) states, *Astron. Astrophys.*, *265*, 850–856, 1992.

Clarke, J. T., J. Ajello, J. Luhmann, N. Schneider, and I. Kanik, Hubble Space Telescope UV spectral observations of Io passing into eclipse, *J. Geophys. Res.*, *99*, 8387–8402, 1994.

Cosby, P. C., Electron-impact dissociation of carbon monoxide, *J. Chem. Phys.*, *98*, 7804–7818, 1993a.

Cosby, P. C., Electron-impact dissociation of nitrogen, *J. Chem. Phys.*, *98*, 9544–9553, 1993b.

Cosby, P. C., Electron-impact dissociation of oxygen, *J. Chem. Phys.*, *98*, 9560–9569, 1993c.

Dunn, G. H., Anisotropies in angular distributions of molecular dissociation products, *Phys. Rev. Lett.*, *8*, 62–64, 1962.

Erdman, P., and E. C. Zipf, Electron impact excitation of the OI 1172.6 Å multiplet, *Planet Space Sci.*, *34*, 1155–1158, 1988.

Feldman, P. D., M. A. McGrath, D. F. Strobel, H. W. Moos, K. D. Retherford, and B. C. Wolven, HST/STIS ultraviolet imaging of polar aurora on Ganymede, *Astrophys. J.*, *535*, 1085–1090, 2000.

Freund, R. S., Dissociation by electron impact of oxygen into metastable quintet and long-lived high-Rydberg atoms, *J. Chem. Phys.*, *54*, 3125–3141, 1971.

Hall, D. T., D. F. Strobel, P. D. Feldman, M. A. McGrath, and H. A. Weaver, Detection of an oxygen atmosphere on Jupiter's moon Europa, *Nature*, *373*, 677–679, 1995.

Hall, D. T., P. D. Feldman, M. A. McGrath, and D. F. Strobel, The far-ultraviolet oxygen airglow of Europa and Ganymede, *Astrophys. J.*, *499*, 475–481, 1998.

Harting, E., and F. H. Read, *Electrostatic Lenses*, 322 pp., Elsevier Sci., New York, 1976.

Itikawa, Y., A. Ichimura, K. Onda, K. Sakimoto, K. Takayanagi, Y. Hatano, M. Hayashi, H. Nishimura, and S. Tsurubuchi, Cross sections for collisions of electrons and photons with oxygen molecules, *J. Chem. Phys. Ref. Data*, *18*, 23–42, 1989.

James, G. K., J. M. Ajello, D. E. Shemansky, B. Franklin, D. Siskind, and T. G. Slanger, An investigation of the second negative system of O_2^+ by electron impact, *J. Geophys. Res.*, *93*, 9893–9902, 1988.

James, G. K., J. M. Ajello, B. O. Franklin, and D. E. Shemansky, Medium resolution studies of EUV emission from N_2 by electron impact: The effect of predissociation on emission cross sections of the $b^1\Pi_u$ state, *J. Phys. B At. Mol. Opt. Phys.*, *23*, 2055–2081, 1990.

Kanik, I., L. W. Beegle, J. M. Ajello, and S. C. Solomon, Electron-impact excitation and photoabsorption cross sections important in the terrestrial airglow and auroral analysis of rocket and satellite observations, *Phys. Chem. Earth, Part C*, *25*, 573–581, 2000.

Lawrence, G. M., Dissociative excitation of some oxygen-containing molecules: Lifetimes and electron-impact cross sections, *Phys. Rev. A Gen. Phys.*, *2*, 397–407, 1970.

Leclair, L. R., Production and detection of metastable atomic oxygen (oxygen), Ph.D. thesis, Univ. of Windsor, Canada, 1993.

Liu, X., S. H. Ahmed, R. Multari, G. K. James, and J. M. Ajello, High-resolution electron-impact study of the far-ultraviolet emission spectrum of molecular hydrogen, *Astrophys. J. Suppl. Ser.*, *101*, 375–399, 1995.

Makarov, O., J. Ajello, I. Kanik, and C. Noren, Electron impact dissociative excitation of O_2: 1. Kinetic energy distributions and Doppler line profiles, *J. Geophys. Res.*, *108*, doi:10.1029/2000JE001422, in press, 2003.

McClintock, W. E., G. M. Lawrence, R. A Kohnert, and L. W. Esposito, Optical design of the ultraviolet imaging spectrograph for the Cassini mission to Saturn, *Opt. Eng.*, *32*, 3038–3046, 1993.

Misakian, M., M. J. Mumma, and J. F. Faris, Angular distributions, kinetic energy distributions, and excitation functions of fast metastable oxygen fragments following electron impact on CO_2, *J. Chem. Phys.*, *62*, 3442–3453, 1975.

Morgan, H. D., and J. E. Mentall, EUV studies of N_2 and O_2 produced by low energy electron impact, *J. Chem. Phys.*, *78*, 1747–1757, 1983.

Mumma, M. J., and E. C. Zipf, Dissociative excitation of vacuum ultraviolet emission features by electron impact of molecular gases: I. H_2 and O_2, *J. Chem. Phys.*, *55*, 1661–1669, 1971.

Noren, C., I. Kanik, J. M. Ajello, P. McCartney, O. P. Makarov, W. E. McClintock, and V. A. Drake, Emission cross section of OI(135.6 nm) at 100 eV resulting from electron-impact dissociative excitation of O_2, *Geophys. Res. Lett.*, *28*, 1379–1382, 2001.

Pang, K. D., J. M. Ajello, B. Franklin, and D. M. Shemansky, Electron impact excitation cross section studies of methane and acetylene, *J. Chem. Phys.*, *86*, 2750–2764, 1987.

Roesler, F. L., et al., Far-ultraviolet imaging spectroscopy of Io's atmosphere with HST/STIS, *Science*, *283*, 353–357, 1999.

Schulman, M. B., F. A. Sharpton, S. Chung, C. C. Lin, and L. W. Anderson, Emission from oxygen atoms produced by electron-impact dissociative excitation of oxygen molecules, *Phys. Rev. A Gen. Phys.*, *32*, 2100–2116, 1985.

Shemansky, D. E., J. M. Ajello, and D. T. Hall, Electron impact excitation of H_2: Rydberg band systems and the benchmark dissociative cross section for H Lyman-α, *Astrophys. J.*, *296*, 765–773, 1985a.

Shemansky, D. E., J. M. Ajello, D. T. Hall, and B. Franklin, Vacuum ultraviolet studies of electron impact of helium: Excitation of He nl P^o Rydberg series and ionization-excitation of He^+ nl Rydberg series, *Astrophys. J.*, *296*, 774–783, 1985b.

Sittler, E. C., and D. F. Strobel, Io plasma torus electrons, *J. Geophys. Res.*, *92*, 5741–5762, 1987.

Torr, M. R., et al., A far ultraviolet imager for the international solar-terrestrial physics mission, *Space Sci. Rev.*, *71*, 329–383, 1995.

Wells, W. C., W. L. Borst, and E. C. Zipf, Absolute cross section for the production of O($^5S^o$) by electron impact dissociation of O_2, *Chem. Phys. Lett.*, *12*, 288–290, 1971.

Zare, R. N., Dissociation of H_2^+ by electron impact: Calculated angular distribution, *J. Chem. Phys.*, *47*, 204–215, 1967.

Zipf, E. C., On the direct and dissociative excitation of the O($3s^3S^o$) state by electron impact on atomic and molecular oxygen, *J. Phys. B At. Mol. Phys.*, *19*, 2199–2209, 1986.

J. M. Ajello, I. Kanik, O. P. Makarov, C. Noren, and P. Vattipalle, Jet Propulsion Laboratory, California Institute of Technology, Pasadena, CA 91019, USA. (jajello@pop.jpl.nasa.gov; ikanik@pop.jpl.nasa.gov; oleg.makarov@uconn.edu; cnoren@jpl.nasa.gov; vattipal@mail.jpl.nasa.gov)

D. E. Shemansky, Department of Aerospace and Mechanical Engineering, 854 W. 36th Place, RRB222, Los Angeles, CA 90089-1191, USA. (dans@hippolyta.usc.edu)